PCCP

ROYAL SOCIETY OF CHEMISTRY

PAPER

View Article Online
View Journal | View Issue

Cite this: *Phys. Chem. Chem. Phys.*, 2022, **24**, 3854

Experimental and theoretical study of adsorption of synthesized amino acid core derived surfactants at an air/water interface

M. Borkowski,[a] S. Orvalho,[b] P. Warszyński,[a] Oleg M. Demchuk,[cd] E. Jarek[a] and J. Zawala *[ae]

The adsorption characteristics of amino acid surfactants, synthesized as substances with different volumes and hydrophilic head properties, have been previously described experimentally, without robust theoretical explanation. A theoretical model enabling the characterization of the adsorption behavior and physicochemical properties of this type of biodegradable surfactants, based on molecular structure, would be beneficial for assessment of their usefulness in colloids and interface science in comparison with typical surface-active substances. In this paper, the adsorption behaviour of synthesized amino acid surfactants at the liquid/gas interface was analyzed experimentally (by surface tension measurements using two independent techniques) and theoretically by means of an elaborate model, considering the volume of the surfactant hydrophilic "head" and its ionization degree. It was shown that the adsorption behavior of the synthesized compounds can be successfully described by the proposed model, including the Helfand–Frisch–Lebowitz isotherm based on the equation of state of 2D hard disk-like particles, with molecular properties of surfactant particles obtained using molecular dynamics simulations (MDS). Model parameters allow for direct comparison of physicochemical properties of synthesized amino acid surfactants with other ionic and non-ionic surface-active substances. Furthermore, it was revealed that intermolecular hydrogen bonds allow the formation of surfactant dimers with high surface activity.

Received 20th November 2021,
Accepted 11th January 2022

DOI: 10.1039/d1cp05322a

rsc.li/pccp

Introduction

Due to the characteristic molecular structure responsible for their surface-active properties, surfactants are widespread in a vast number of important industrial and technological applications and everyday human life. They are widely used as detergents, foaming enhancers, emulsifiers, wettability modifiers, and coating agents in many different fields such as detergency, fibers, food, polymers, pharmaceuticals, the pulp-paper industry, as corrosion inhibitors as well as in mineral processing and oil recovery applications.[1–3] In most applications, synthetic surfactants are used, and their production, which exceeds millions of tons per year, is cheap and well optimized. On the other hand, usage of such large quantities of surface-active substances in industry and households is one of the greatest sources of environmental pollution (60 wt% of total surfactants produced enters the aquatic environment[3,4]). Due to environmental concerns, the potential replacement of synthetic surfactants by environment-friendly alternatives is extensively investigated.[3,5,6]

To replace conventional surfactants, new "green" compounds must retain functional properties while simultaneously reducing their environmental impact. One of the groups of compounds having the potential to become superior to conventional surfactants are amino acid surfactants (AASs). These are simple compounds with tunable features and great potential as sustainable, low toxicity and biodegradable substances. AASs properties depend on their synthesis path. Suitable, properly chosen synthesis pathways allow for AASs' extensive structural diversity affecting their physicochemical properties,[2] determining the sites of alkyl chain substitution (*N*-substituted, *C*-substituted, or both *N*- and *C*-substituted compounds) and the number of attached chains (linear chain, Gemini, and bolaamphiphile forms). The type of proteinogenic amino acids chosen for the synthesis determines the final product polarity, adsorption features, surface activity and acid–base behavior.[2,7–9]

The search for environment-friendly surfactants requires their thorough characterization, including the determination

[a] *Jerzy Haber Institute of Catalysis and Surface Chemistry Polish Academy of Sciences, ul. Niezapominajek 8, 30-239 Krakow, Poland. E-mail: jan.zawala@ikifp.edu.pl*
[b] *Institute of Chemical Process Fundamentals, Czech Academy of Sciences, Rozvojova 135/1, 165 02 Prague 6, Suchdol, Czech Republic*
[c] *Faculty of Science and Health, The John Paul II Catholic University of Lublin, 1h-Konstantynów St., 20-708 Lublin, Poland*
[d] *SBŁ-Pharmaceutical Research Institute, 8-Rydygiera St., 01-793 Warsaw, Poland*
[e] *Department of Chemical Engineering, Stanford University, 443 Via Ortega, Shriram Center, Stanford, CA 94305, USA*

of molecular structure and surface activity. This paper presents the analysis of the adsorption behavior of five AASs based on alanine, valine, leucine, proline, and phenylalanine, with an amide bond connecting the polar head-group (originating from natural amino acids) and a hydrophobic tail (originating from lauric acid, a natural fatty acid). The adsorption of the synthesized compounds at the liquid/gas interface is analyzed experimentally and a theoretical model is proposed for AASs adsorption behavior and surface activity. The model integrates the results of molecular dynamics of surfactant molecules at the interface with the conventional description of the adsorption in terms of the surface tension isotherm. The proposed model uses the HFL (Helfand–Frisch–Lebowitz) isotherm based on the equation of state of 2D hard disk-like particles, with the effective headgroup size obtained using molecular dynamics simulations (MDS). Applying DFT (density functional theory) computations, we also demonstrate that intermolecular hydrogen bonds between amide groups of surfactants can contribute to the formation of dimers that affects the surface activity of the investigated surfactants.

Materials and methods

Chemicals

All the amino acid surfactants (AASs) studied in this paper were synthesized by condensation of proper amino acid (L-alanine, L-valine, L-leucine, L-proline, and L-phenylalanine) with dodecanoyl (lauroyl) chloride (Fig. 1), obtained from the reaction of lauric acid with thionyl chloride. The synthesis details are described in Appendix A. The chemicals used in the synthesis of lauroyl chloride and of the final products were purchased from Avantor Performance Materials Poland S. A. and Merck KGaA. The solutions of synthesized surfactants used in the study were prepared with ultrapure water (Direct-Q3 UV Water Purification System by Millipore, conductivity <0.7 μS cm^{-1} and surface tension equals 72.4 mN m^{-1} at 22 °C).

The structural formulas of five surfactants with different hydrophilic heads (amino acid), namely: *N*-lauroyl-L-alanine (C12-ALA), *N*-lauroyl-L-valine (C12-VAL), *N*-lauroyl-L-leucine (C12-LEU), *N*-lauroyl-L-proline (C12-PRO), and *N*-lauroyl-L-phenylalanine (C12-PHE), are shown in Appendix B, together with the results of the purity analysis of the synthesized compounds. The purity of the AASs was verified by NMR spectra, and by the melting point (Mp.) determination. ^{1}H NMR (500 MHz) and ^{13}C NMR (125 MHz) spectra were recorded on a Bruker AVANCE 500 MHz spectrometer using $CDCl_3$ (deuterated chloroform) as a solvent. All the physical and spectral data of the synthesized AASs was consistent with those found in literature[10,11] and are listed in Appendix B.

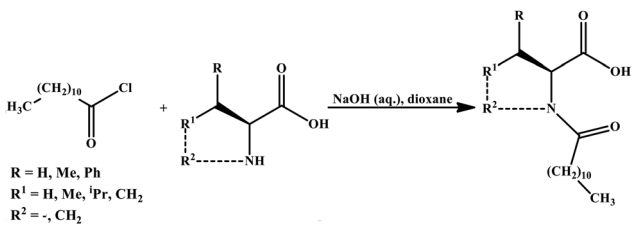

Fig. 1 Synthesis of the amino acid surfactants (AASs).

Methods

All measurements of interfacial and bulk physicochemical properties of the AASs were carried out at controlled temperature (21 ± 1 °C). Standard cleaning procedures were followed before each measurement, including careful cleaning of the sample vessel with a cleaning agent (Mucasol – a commercially available laboratory cleaning liquid) and thorough rinsing with ultrapure water. In a typical experimental run, the surfactant solution of a given concentration was tested according to the following sequence: (i) determination of equilibrium value of surface tension, (ii) determination of solution pH, and (iii) its conductivity.

Equilibrium surface tension measurements

Equilibrium values of surface tension were measured using two independent methods: (i) Wilhelmy plate method in a Krüss Tensiometer, Type K11 and (ii) bubble shape method in PAT-1 tensiometer (SINTERFACE Technologies, Berlin, Germany). In the Wilhelmy plate technique, a standard platinum plate (wetted perimeter 40.198 mm) and 60 mL solution were used for each measurement. The surface tension of the solution was measured for 1000 s, recorded at 2-second intervals. Equilibrium surface tension for a given solution concentration was calculated as the average from the values being constant in time. In the bubble shape method, the surface tension values were determined by analyzing the shape of a submerged bubble attached to a U-shaped needle. The Young–Laplace equation, relating the curvature of a liquid meniscus and its surface tension, was fitted to describe the bubble shape. The surface tension in this case was measured for 2 h, and the equilibrium surface tension values were calculated accordingly.

Solution pH and conductivity determination

The conductivity and pH of the tested solutions were measured using a WTW conductometer, Type LF 330i, with probe Tetra-Con 325, covering a conductivity range: 0.1 μS cm^{-1} –2 S cm^{-1}, and a WTW pH meter, Type 340i, with probe SenTix 41. Before each series of measurements, the measuring electrodes were thoroughly rinsed with ultrapure water (reference values: pH $\sim$5.8 and conductivity $\sim$0.7 μS cm^{-1}).

Determination of the acid dissociation constant

The values of the acid dissociation constant K_A were determined by the weak acid titration method, using NaOH solution as a strong base.[12] Detailed experimental and data evaluation procedures are described in Appendix C. The titration procedure was monitored independently by pH and conductivity measurements using an Elmetron CPS-505 pH/conductivity meter equipped with the electrode Elmetron EPS-1 for measuring pH and an Elmetron EC-60 for measuring conductivity.

Theoretical description of the adsorption process – adsorption isotherm

The HFL (Helfand–Frisch–Lebowitz) isotherm based on the equation of state of 2D hard disk-like particles[13] was used to describe the synthesized AASs adsorption at the water/air interface. That exact equation for the 2D equation of state can also be derived based on the scaled particles theory[14] and extended to mixtures of hard disks with various diameters.[15] Accounting for the intermolecular interactions in the adsorbed layer in the Frumkin-like manner[16] and applying the Gibbs adsorption equation for the adsorption equilibrium,[17] the equation for the adsorption isotherm was obtained in the form:

$$\frac{c_n}{\alpha_n}(1-\theta_n)\exp\left[\frac{2\theta_n^2-3\theta_n}{(1-\theta_n)^2}\right]=\theta_n\exp(-2H_s\theta_n/RT) \quad (1)$$

where: c_n is the concentration of surfactant, α_n is the surface activity of the surfactant, a measure of the standard free energy of adsorption, $\theta_n = \Gamma_n/\Gamma_{n\infty}$ is the relative surfactant surface concentration, where Γ_n is surface concentration, while $\Gamma_{n\infty}$ is the limiting surfactant surface concentration of the closely packed monolayer and H_s is the surface interaction parameter, accounting mainly for the attractive lateral intermolecular interaction between adsorbed surfactant molecules (*e.g.* London dispersion, dipole–dipole, hydrogen bonding). In the scaled particles theory, the limiting surface concentration is directly dependent on the size of the hard disk:

$$\Gamma_{n\infty}=\frac{1}{N_A\pi A_{eff}^2} \quad (2)$$

where: N_A is the Avogadro constant and A_{eff} is the hard disk radius. By the numerical solution of eqn (1), the dependence between relative surface concentration of surfactant and its concentration in the bulk was found and the surface tension isotherm was described by the integration of the Gibbs equation for a diluted solution of non-ionic surfactant:

$$d\gamma=-RT\frac{\Gamma_n}{c_n}dc_n \quad (3)$$

The calculated isotherm can be fitted to the experimental data with three fitting parameters (A_{eff}, α_n, H_s) to obtain the parameters of the model for a given AASs with different amino acid head group. The quality of the fit was evaluated based on the χ^2 value defined as:

$$\chi^2=\sum_{i=1}^{n_e}\frac{(\gamma_e-\gamma_f)^2}{n_e} \quad (4)$$

where: γ_e and γ_f are the experimental and fitted values of surface tension, and n_e is the number of experimental points for a given isotherm.

To assign physical meaning to the isotherm parameters with respect to the molecular properties of the studied surfactants, molecular dynamics simulations (MDS) were used to determine the effective size of the surfactants' hydrophilic part, A_{eff}, that can be used in the eqn (1) and (2). The following procedure was applied:

- The optimized structures of all AASs were obtained by quantum mechanics computations, using density functional theory (DFT) with CAM–B3LYP functional and 6-31G + (d, p) basis set. Solvation effects (water) were accounted for applying the SMD (solvation model) variation of the Polarizable Continuum Model,[18] while the partial atomic charges were calculated according to the Merz–Singh–Kollman method.[19] All DFT calculations were carried out using the Gaussian 09 program.[20]
- The optimized structure, obtained in the previous step, was imported to the YASARA Structure Molecular Dynamics Software,[21] placed in the simulation box with the size of 6 × 6 × 3.5 nm and filled with water molecules (TIP3P, density 1 g dm^{-3}). The simulation was run for 20 ns using AMBER 14 force field[22] to equilibrate the system.
- Next, the simulation box was extended in the z coordinate to 12 nm to obtain a water slab with two interfaces. When the simulations were running, the transfer of a surfactant molecule to one of the interfaces was observed.

The simulations were continued for 35 ns, and at least ten snapshots were randomly taken. Representative snapshots for all the AASs are illustrated in Fig. 2. The conformation of the surfactant at the interface was analyzed at every snapshot and the hydrophilic headgroup of the surfactant that preferentially contacted with water sub-phase was determined (marked by the grayish contour in Fig. 2).

Fig. 3. shows the optimized structures of surfactants with marked hydrophilic parts of molecules. The effective radii of the hydrophilic part of surfactants were determined using the formula:

$$A_{eff}=\frac{3V}{S} \quad (5)$$

where V is the van der Waals volume of the hydrophilic head group shown in Fig. 3. and S is the respective van der Waals surface. Their values and the radii of gyrations of surfactant headgroups were calculated using algorithms implemented in the YASARA Structure software.[21] The A_{eff} were then used in eqn (1) for the fitting to the experimentally obtained adsorption isotherms. Therefore, the number of adjustable parameters in eqn (1) was

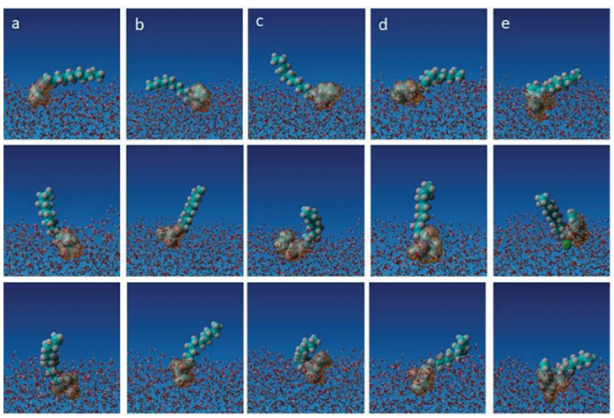

Fig. 2 Example of results obtained by molecular dynamic simulations: selected snapshots of amino acid surfactant molecule at air/water interface respectively for (a) C12-ALA (b) C12-VAL, (c) C12-LEU, (d) C12-PRO, (e) C12-PHE.

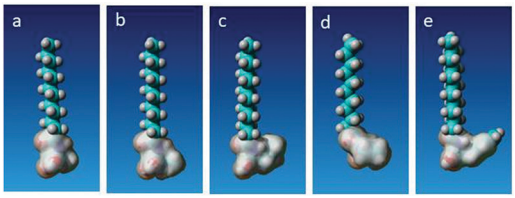

Fig. 3 Optimized geometries of amino acid surfactants for (a) C12-ALA (b) C12-VAL, (c) C12-LEU, (d) C12-PRO, (e) C12-PHE. The van der Waals surface of the hydrophilic headgroup is marked by the grayish contour.

reduced to two, α_n and H_s, as the third one, A_{eff}, could be determined independently.

Energy of dimerization

The minimized structures of AASs dimers were obtained by quantum mechanics computations, using density functional theory (DFT) with wB97XD functional, which includes corrections for the London dispersion and long-range interactions, using 6-31G + (d,p) basis set. Solvation effects (water), as above, were accounted for applying the SMD variation of the Polarizable Continuum Model. The calculations started by placing two molecules with minimized geometries with parallel oriented hydrophobic chains and random orientation of the headgroup. Then the optimizing procedure was run until convergence was achieved and the energy and free energy of the dimer were obtained. The optimizing procedure was repeated three times for different initial orientations of headgroups and the conformation with the lowest energy was selected. The energy, enthalpy, and free energy of dimerization were calculated according to: $\Delta E_{dimerization} = E_{dimer} + 2E_{surfactant}$. All calculations were carried out using the Gaussian 09 program.[20]

Results and discussion

To verify and validate our theoretical description of surfactant adsorption at the air/water interface, we selected literature data on surface tension isotherms of model non-ionic surfactants, namely *tert*-isopropyl phosphine oxide[23] and *n*-alkyl dimethyl phosphine oxides[24] with the hydrophobic chain length from 7 to 13 carbon atoms. The surface tension isotherms for those model surfactants are illustrated in Fig. 4, together with fits of the theoretical model based on their molecular size. The best-fit parameters are resumed in Table 1. *Tert*-isopropyl phosphine oxide is a disk-like molecule; therefore, it seems to be a perfect model surfactant to verify the HFL model for the hard disk based on its molecular size. Due to its branched structure, its surface activity is low, with no lateral interactions between adsorbed molecules ($H_s = 0$).[23] After determining the effective size from the molecular data ($A_{eff} = 0.248$ nm), we could perfectly describe the experimental surface tension isotherms with only one adjustable parameter. For the homologous series of *n*-alkyl dimethyl phosphine oxides, we successfully fit the model with a single size of the headgroup (marked in Fig. 4B) and two adjustable parameters, α_n and H_s. The logarithm of the first one exhibits a linear dependence on the number of carbon atoms in the hydrophobic chain, in agreement with the Traube rule. The second one, H_s, shows the odd–even effect in the hydrocarbon chain length as described in.[24]

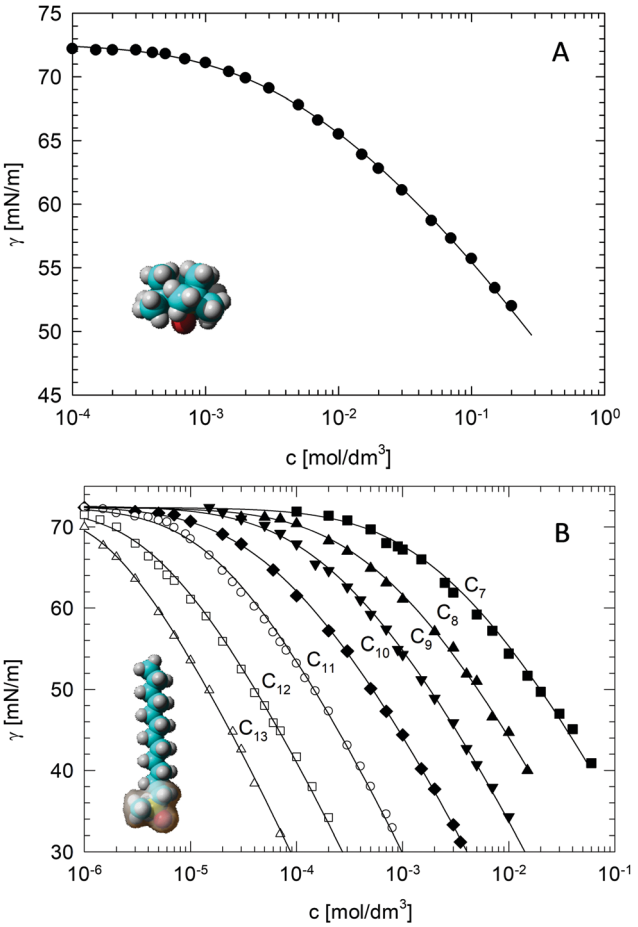

Fig. 4 Surface tension isotherms and molecular structures of: A – *tert*-isopropyl phosphine oxide and B – *n*-alkyl dimethyl phosphine oxides. Lines represent fits of the theoretical model.

Table 1 The effective diameter and the best-fit parameters of the theoretical model, based on the molecular dimensions, to the experimental isotherms of model surfactants. Adjustable parameters in bold

Surfactant	A_{eff} [nm]	α_n [mol dm^{-3}]	H_s [kJ mol^{-1}]	χ^2 [(mN m^{-1})^2]
Tert-isopropyl phosphine oxide	0.334	5.5×10^{-3}	0.0	0.02
N-alkyl dimethyl phosphine oxide				
C_7	0.248	2.90×10^{-3}	0.0	0.50
C_8		8.00×10^{-4}	0.3	0.26
C_9		3.00×10^{-4}	0.9	0.21
C_{10}		9.00×10^{-5}	1.2	0.07
C_{11}		4.50×10^{-5}	4.5	0.23
C_{12}		1.35×10^{-5}	4.9	0.24
C_{13}		7.70×10^{-6}	7.4	0.26

After the initial validation, the model was used to describe the adsorption performance of the synthesized AASs. In contrast to amino acids, AASs do not assume a zwitterionic form at moderate pH. They behave as weak acids with pK_a determined

Table 2 Experimentally determined pK_a values of the studied amino acid surfactants

No.	surfactant	pK_a
1	C12-ALA	4.63
2	C12-VAL	5.13
3	C12-LEU	5.41
4	C12-PHE	5.40
5	C12-PRO	4.61

by the protonation of a carboxylic group. The experimentally determined pK_a values of all studied AASs surfactants are presented in Table 2. Based on these pK_a values and on the measured pH of the surfactants' solutions, the dependence of the degree of dissociation (α) on their concentration was determined using the mass action law:

$$\alpha(c) = \frac{K_A}{K_A + 10^{-\mathrm{pH}(c)}} \quad (6)$$

where K_A is the dissociation constant of the carboxylic group of the surfactants and c is the total concentration of surfactant in the solution. The results are illustrated in Fig. 5, where the dependence of the fraction of non-dissociated surfactant ($1 - \alpha(c)$) on total surfactant concentration is given (solid line) together with the experimentally determined dependence of pH.

As illustrated in Fig. 5, the fraction of the non-dissociated form of surfactant is always above 0.1. In our previous studies,[25,26] we demonstrated that non-ionic surfactants with the same hydrocarbon chain are much more surface active than the respective ionic ones, and the difference in concentration of the onset of surface activity was near two orders of magnitude. This feature in particular was revealed when analyzing the pH dependence of the surface activity of alkanoic acids.[27] Therefore, in the analysis of surface tension isotherms of the studied AASs, we neglected the effect of ionic (dissociated) surfactant form and considered non-ionic form only, with the concentration given by:

$$c_n = c[1 - \alpha(c)] \quad (7)$$

where c is the total surfactant concentration. The equation of the adsorption isotherm (eqn (1)) used to describe the AASs system could be rewritten as:

$$\frac{c[1-\alpha(c)]}{a_n}(1-\theta_n)\exp\left[\frac{(2\theta_n^2 - 3\theta_n)}{(1-\theta_n)^2}\right] = \theta_n \exp\left(-\frac{2H_s\theta_n}{RT}\right) \quad (8)$$

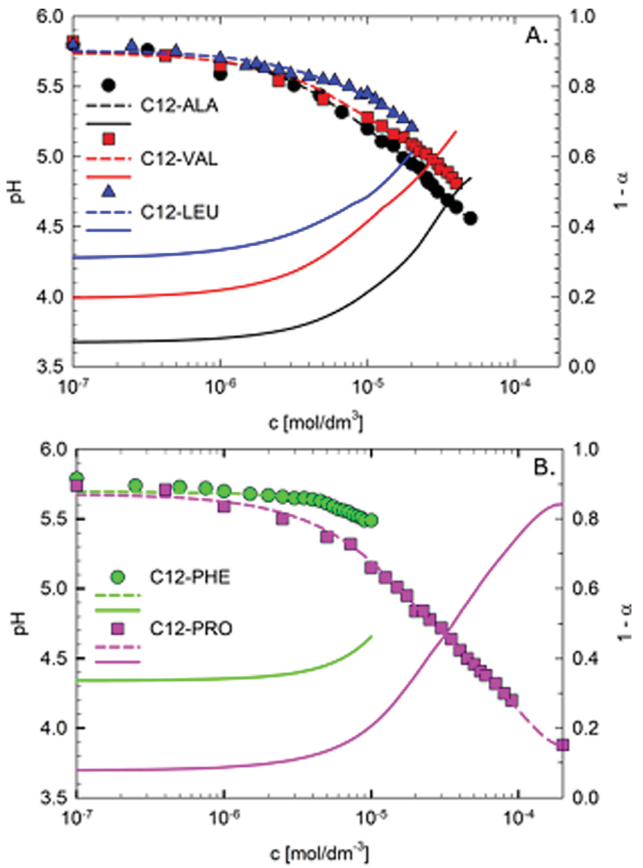

Fig. 5 Experimentally determined dependence of the pH of the solution on the concentration of amino acid surfactants (symbols, dashed line) for: (A) C12-ALA, C12-VAL, C12-LEU; (B) C12-PRO, C12-PHE. The respective dependence of the fraction of non-dissociated surfactant calculated using eqn (6). is shown as solid lines.

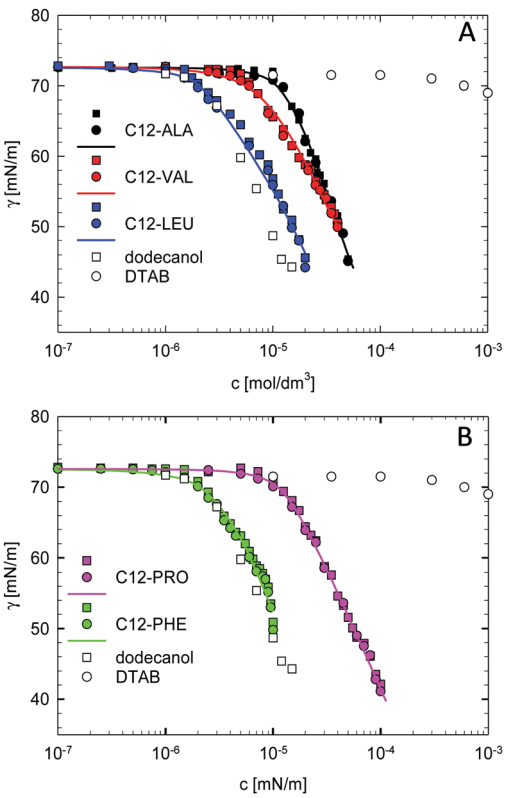

Fig. 6 Experimental surface tension isotherms of the amino acid surfactants (determined by Wilhelmy plate method – squares, bubble shape analysis – circles) for (A) C12-ALA, C12-VAL, N-C12-LEU; (B) C12-PRO, C12-PHE. Solid lines – best fits of the theoretical model to experimental points obtained using bubble shape analysis method. The experimental isotherms for dodecanol and DTAB are given for comparison.

Table 3 Calculated and best-fit parameters of the theoretical model fitted to the experimental adsorption isotherms (fitted parameters in bold)

Parameter	C12-ALA	C12-VAL	C12-LEU	C12-PHE	C12-PRO
A_{eff} [nm]	0.257	0.276	0.284	0.280	0.272
Rg_{hg}[nm]	0.204	0.233	0.256	0.241	0.231
$\Gamma_{n\infty}\cdot10^{-10}$ [mol cm^{-2}]	8.002	6.938	6.553	6.741	7.144
$\alpha_n\cdot10^{-5}$ [mol dm^{-3}]	4.2 ± 0.2	2.0 ± 0.2	0.86 ± 0.05	0.77 ± 0.05	2.0 ± 0.2
H_s [kJ mol^{-1}]	14.3 ± 0.4	11.3 ± 0.3	13.2 ± 0.4	13.4 ± 0.4	10.0 ± 0.4
χ^2 [(mN m^{-1})^2]	0.38	0.15	1.23	1.37	0.61

The experimental surface tension isotherms for the investigated AASs are illustrated in Fig. 6, together with the best fits of the theoretical model. Results obtained using two experimental methods, Wilhelmy plate (squares) and bubble shape analysis (circles), are presented. Almost perfect agreement between the two sets of data (indicating lack of diffusion limitation effects that may occur in surface tension measurements at low surfactant concentrations[28]) was revealed.

The effective radii of the hydrophilic headgroups of the surfactants, A_{eff}, and the limiting surface concentration, $\Gamma_{n\infty}$, were calculated based on the MDS procedure and - eqn (2) and (5), respectively, using van der Waals volumes of the hydrophilic headgroups (*cf.* Fig. 3). All the calculated and fitted isotherm parameters are presented in Table 3. The effective radii of the headgroups were *ca.* 0.4 Å bigger than their respective radii of gyration (Rg_{hg}). The fits to experimental surface tension isotherm were obtained with two adjustable parameters only, α_n and H_S.

The obtained results revealed that, as could be expected, the surfactants' surface activity increases (α_n parameter decreases) with the hydrophobicity of the amino acid side group: *N*-Lauroyl L-phenylalanine having benzene ring is more surface active than *N*-Lauroyl L-proline with more hydrophilic pyrrolidine loop. Moreover, the surface activity of AASs follows the gradation of hydrophobicity of amino acids PRO < ALA < VAL < LEU < PHE[29] and it is much higher than the one of a typical cationic surfactant with twelve carbon atoms in the alkyl chain -- dodecyltrimethylammonium bromide (DTAB), which has the onset of surface activity at the concentration 10^{-3} mol dm^{-3} (the studied AASs have surface activity onset at concentrations below 10^{-4} mol dm^{-3}) and the critical micelle concentration (CMC) above 10^{-2} mol dm^{-3}. The surface activities of C12-PHE and C12-LEU were similar to dodecanol (*cf.* Fig. 6), while those of C12-VAL, C12-ALA and C12-PRO were in-between the one of dodecanol and dodecyl-trimethyl ammonium bromide (DTAB). That is due to increasing both hydrophobicity of the amino acid headgroup and the fraction of the neutral form of the molecule with a protonated carboxylic group.

The calculated dependencies of surface concentration *versus* surfactant concentration in volume for the studied AASs are illustrated in Fig. 7. The investigated surfactants do not have a CMC at room temperature and their surface activity is limited by solubility. At the surfactant concentration corresponding to the respective solubility limit, the surface concentrations range from 4.6 × 10^{-10} mol cm^{-2} for C12-ALA to 3.7 × 10^{-10} mol cm^{-2} for C12-PHE and are much smaller than the ones determined by the effective molecular dimensions of surfactant headgroups (*cf.* Table 3).

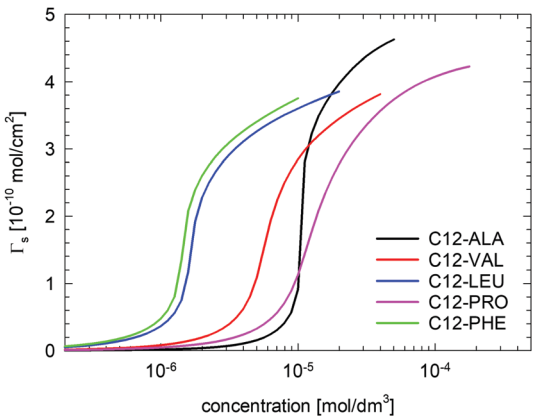

Fig. 7 The calculated dependence of surface concentration *vs.* bulk concentration resulting from the fitting of the model to the experimental surface tension isotherms.

The proposed theoretical model describes the experimental results very well with the χ^2 less than 1, except for C12-LEU and C12-PHE. The AASs are capable of making hydrogen bonds (HB).

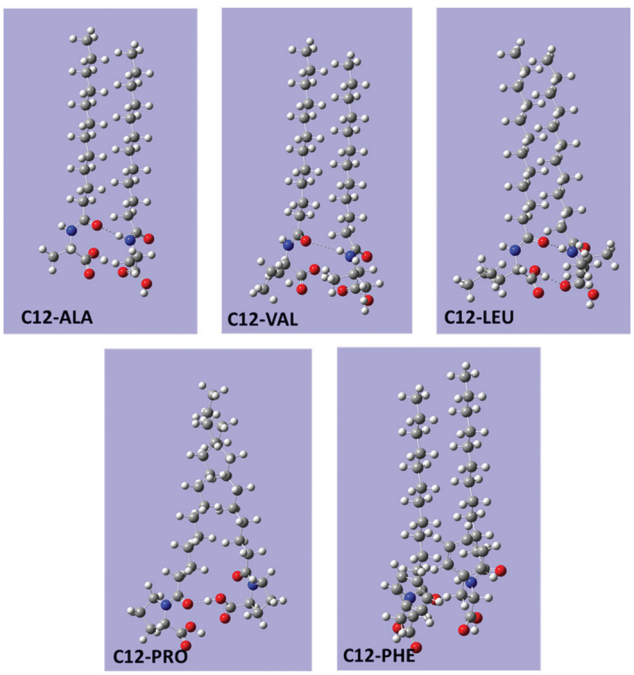

Fig. 8 The optimized structures of AAS dimers resulting from the DFT calculations.

Table 4 The energy, enthalpy and free energy of dimerization resulting from DFT computations

Surfactant	Energy of dimerization [kcal mol^{-1}]	Enthalpy of dimerization [kcal mol^{-1}]	Free energy of dimerization [kcal mol^{-1}]
C12-ALA	23.07	23.66	3.71
C12-VAL	21.07	21.67	0.79
C12-LEU	24.72	25.31	5.53
C12-PHE	27.11	27.70	5.43
C12-PRO	18.30	18.89	1.29

The C12-ALA, C12-VAL, C12-LEU, C12-PHE have 3 HB acceptors (oxygen in carboxylic and amide group) and 2 donors (hydrogens of carboxylic and amide group), while C12-PRO has 3 HB acceptors (oxygen in carboxylic and amide groups) but only 2 donors in carboxylic group. Due to competition with water molecules, the carboxylic groups preferably participate in hydrogen bonds with hydration water. On the other hand, the amide group is adjacent to the hydrophobic tail and more exposed to the gas phase (*cf.* Fig. 2). Thus, at high surface coverage, it can form intermolecular hydrogen bonds. We attempted to evaluate the energy of dimerization for all AASs by performing the optimization geometry of the dimers. The resulting structures of the dimers are illustrated in Fig. 8, and the values of the energy, enthalpy and free energy of dimerization are given in Table 4. The determined free energy of dimerization was the highest for C12-LEU and C12-PHE and the lowest for C12-VAL and C12-PRO that agrees with the shape of surface tension isotherms. Strong intermolecular interactions can be evidenced by a high values of interaction parameter, H_s (*cf.* Table 3) for C12-ALA, C12-LEU and C12-PHE. Those values are much higher than for phosphinoxides despite similar size of the bulky headgroups (*cf.* Table 1). The latter are mainly determined by the dispersion interaction between hydrocarbon chains at the interface. For C12-PRO, the hydrogen bond can form between amide oxygen and the hydrogen of the carboxylic group that is entropically unfavorable.

As can be observed in Fig. 6, for C12-LEU and C12-PHE the end part of the isotherms, close to the solubility limit, is characterized by a steep slope. That can be a manifestation of the formation of highly surface-active dimers stabilized by hydrogen bond and for phenylalanine-based surfactant, additionally by a π–π stacking.[30]

Conclusions

Amino acid surfactants are biodegradable compounds with promising adsorption properties competitive to typical surface-active substances.[2,5,32] Although their ability to reduce solution surface tension is presented in many papers,[5,9,32–34] there is an acute lack of reported attempts for the robust theoretical description of the adsorption process by means of a model, allowing extraction of useful physicochemical parameters of the studied compounds. Our studies aim to fill this gap. Five amino acid based surfactants (AASs), derived from L-alanine, L-valine, L-leucine, L-proline, and L-phenylalanine, were successfully synthesized. The synthesized AASs present an amide bond connecting the polar head-group to a lipophilic lauroyl tail. The solutions of AASs at natural pH (*i.e.*, without any pH adjustments) contain both deprotonated, anionic and protonated non-ionic forms. Since, according to previous studies,[27] the non-ionic forms are much more surface active, their presence dominates the interfacial behavior. Therefore, the AASs adsorption isotherms could be successfully characterized by a theoretical model, based on the Helfand–Frisch–Lebowitz isotherm derived from the equation of state of 2D hard disk-like particles. The effective sizes of the hydrophilic headgroups of the AASs were obtained by molecular dynamics simulation and the adsorption isotherms were fitted by adjusting only two parameters, the surface activity of the surfactant and the surface interaction parameter. The new AASs show higher efficiency of adsorption (lower pC20[35]) than typical ionic surfactants (Table 5) but lower than rhamnolipids.[36] Their surface activity is comparable with non-ionic Triton or Tween,[37,38] and relative surface activity correlates with increasing hydrophobicity of the amino acid (Table 6). The use of the new AASs in typical surfactant applications is promising and the testing of other desired properties will follow: foamability tests, determination of the kinetics of dynamic adsorption layer formation at the interface of rising bubbles, stability of single liquid film, as well as studies of the crystalline structure of the obtained AASs to understand the AASs dimerization.

Table 5 Comparison of the efficiency of adsorption of the new AASs with ionic surfactants with lipophilic lauroyl tail

	New AASs	DTAB[26]	SDS[26]
pC_{20}	4.55–5.1	2.00	2.50

List of symbols and abbreviations.

c_n	The concentration of surfactant's form adsorbed at liquid/gas interface
c	The total concentration of surfactant
α_n	Surface activity of the surfactant being the measure of the standard free energy of adsorption
Γ_n	Surface concentration
$\Gamma_{n\infty}$	Limiting surfactant surface concentration of the closely packed monolayer
θ_n	Relative surfactant surface concentration
H_s	Surface interaction parameter approximating the attractive lateral interaction among the adsorbed surfactant hydrophobic tails
A_{eff}	Effective radii of the hydrophilic head of surfactants
V	van der Waals volume of hydrophilic head group of surfactants

Table 6 Relative hydrophobicity of the investigated amino acids and the efficiency of adsorption and surface activity of their respective AASs

Amino acid	Phe[a]	Leu	Val	Ala	Pro[b]
Hydrophobicity[31]	2.00	1.68	1.11	0.15	−0.25
pC_{20}	5.10	4.95	4.65	4.60	4.55
$\alpha_s \times 10^{-5}$ [mol dm^{-3}]	0.77	0.86	2.0	3.9	1.5

[a] most hydrophobic. [b] least hydrophobic.

S	van der Waals surface of hydrophilic head group of surfactants
γ	Surface tension of solution
α	Dissociation degree
K_A	Dissociation constant of carboxylic group of the surfactant
χ	Measure of the difference between the model prediction and the experimental data
N_A	Avogadro constant
pC_{20}	Negative log of the bulk phase concentration necessary to reduce the surface tension by 20 mN m^{-1}
Rg_{hg}	Radius of gyration
R	Gas constant
T	Temperature
AASs	Amino acid surfactants
DFT	Density functional theory
MDS	Molecular dynamics simulations
SDM	Solvation model density
DMF	Dimethylformamide
TMS	Tetramethylsilane
C12-ALA	*N*-lauroyl-L-alanine
C12-VAL	*N*-lauroyl-L-valine
C12-LEU	*N*-lauroyl-L-leucine
C12-PRO	*N*-lauroyl-L-proline
C12-PHE	*N*-lauroyl-L-phenylalanine

Conflicts of interest

There are no conflicts to declare.

Appendix A (Synthesis of Lauroyl chloride and Amino acid surfactants)

Lauroyl chloride

300 mL of toluene, 0.5 mL of DMF (dimethylformamide) and 43 g of lauric acid (0.22 mol) were placed into the 500 mL round bottom flask equipped with a magnetic stirrer and a reflux condenser with a pipe for gas trapping of HCl (hydrochloric acid) and SO_2 (sulphur dioxide) produced in the reaction. 31 mL of $SOCl_2$ (0.44 mol) was added to the mixture, which was gently stirred. The mixture stirring was continued for 10 h, in mild reflux conditions, heated in the oil bath. The liberated gases were absorbed with sodium hydroxide solution. After completing the reaction, the reflux condenser was replaced with an adapter for simple distillation, and the majority of the solvent (about 250 mL) was distilled at ambient pressure. The remaining solvent was distilled under the vacuum at a temperature below 100 °C. The obtained lauroyl chloride was used in the AASs syntheses without additional purification.

***N*-Lauroyl-L-alanine (typical procedure)**

A 250 mL round bottom flask equipped with a magnetic stirrer, dropping funnel, placed in an ice bath, was charged with L-alanine (4 g, 0.045 mol) and 30 mL of dioxane. A solution of NaOH (sodium hydroxide, 3.9 g, 0.098 mol) in 30 mL of water was slowly added to the stirred slurry, while the temperature was maintained at +5 °C. The solution of lauroyl chloride (10 g, 0.046 mol) in 30 mL of dioxane was slowly added to the stirred solution of freshly obtained sodium alaninate, maintaining the reaction temperature below +5 °C. The stirring at that temperature was prolonged for one more hour, and for the next 16 hours at ambient temperature, then 20 mL 12% HCl was added. The organic phase was diluted and separated with 50 mL of ^{t}BuOMe (methyl *tert*-butyl ether), washed with 30 mL of 2M HCl, and 30 mL of water, then dried with anhydrous $MgSO_4$ (magnesium sulfate). The drying agent was removed by filtration, solvents evaporated off under reduced pressure of rotary evaporator, and the product was purified by crystallisation from the mixture heptane/^{t}BuOMe to yield 8.5 g (71%) of product.

N-Lauroyl-L-leucine was prepared according to the typical procedure. The product was purified by crystallisation from the mixture hexane/toluene/DCM to yield 64% of the product.

N-Lauroyl-L-proline was prepared according to the typical procedure. The product was purified by crystallisation from the mixture hexane/toluene to yield 86% of the product.

N-Lauroyl-L-valine was prepared according to the typical procedure. The product was purified by crystallisation from the mixture hexane/toluene to yield 79% of the product.

N-Lauroyl-L-phenylalanine was prepared according to the typical procedure. The product was purified by crystallisation from the mixture hexane/toluene/DCM to yield 82% of the product.

Appendix B (Purity analysis and chemical structure of the synthesized amino acid surfactants)

Melting points (Mp.) were determined in open capillaries and are given as uncorrected values. The chemical shifts are reported in ppm, and calibrated to residual solvent peaks at 7.27 ppm and 77.00 ppm for ^{1}H and ^{13}C, respectively, or 0.00 ppm for TMS (tetramethylsilane) used as internal reference compounds (Fig. 9–13).

***N*-Lauroyl-L-alanine (C12-ALA)**

Mp. = 85.0–86.0 °C.

^{1}H NMR (500 MHz, $CDCl_3$): δ = 10.03 (bs, 1H), 6.28 (bd, J = 6.9 Hz, 1H), 4.59 (q, J = 7.1 Hz, 1H), 2.25 (t, J = 7.6 Hz, 2H), 1.63 (bq, J = 6.6 Hz, 2H), 1.46 (d, J = 6.9 Hz, 3H), 1.35–1.22 (m, 17H), 0.88 (t, J = 6.6 Hz, 3H). ^{13}C NMR (DEPT, 125 MHz, $CDCl_3$): δ = 48.26, 36.45, 31.91, 29.60, 29.47, 29.33, 29.30, 29.18, 25.58, 22.69, 18.11, 14.11.

***N*-Lauroyl-L-valine (C12-VAL)**

Mp. = 97.0–99.2 °C.

^{1}H NMR (500 MHz, $CDCl_3$): δ = 9.23 (bs, 1H), 6.12 (d, J = 8.5 Hz, 1H), 4.60 (dd, J = 8.5 Hz, 1H), 2.29–2.22 (m, 3H), 1.64 (q, J = 7.1 Hz, 2H), 1.35–1.25 (m, 16H), 0.99 (d, J = 6.9 Hz, 3H), 0.96 (d, J = 6.6 Hz, 3H), 0.88 (t, J = 6.9 Hz, 3H). 13C NMR (125 MHz,

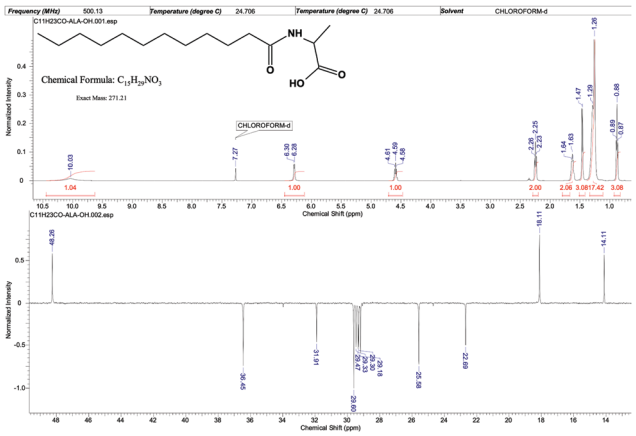

Fig. 9 The NMR spectrum of *N*-Lauroyl-L-alanine (C12-ALA).

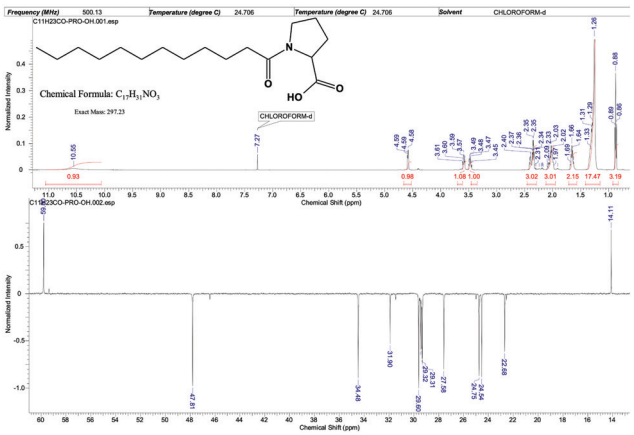

Fig. 12 The NMR spectrum of *N*-Lauroyl-L-proline (C12-PRO).

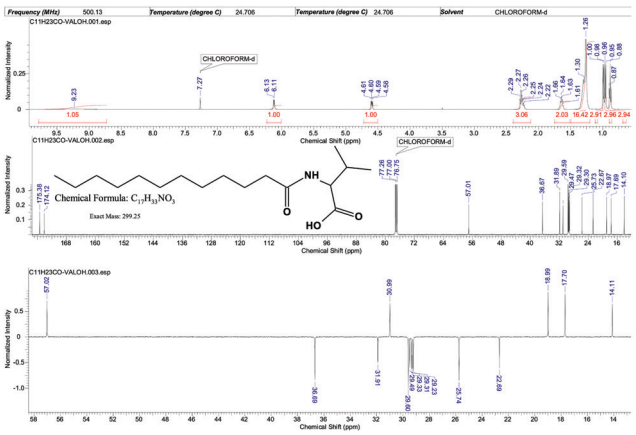

Fig. 10 The NMR spectrum of *N*-Lauroyl-L-valine (C12-VAL).

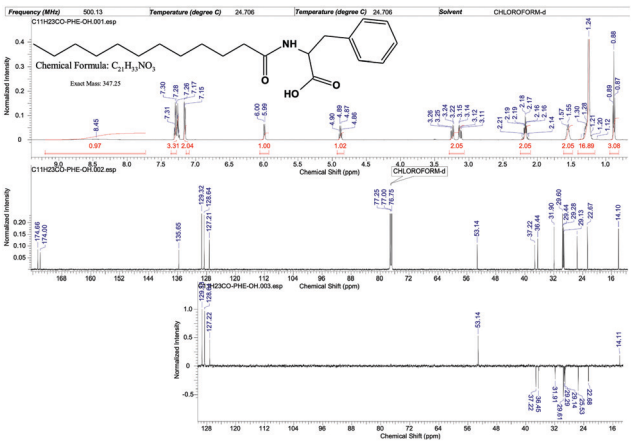

Fig. 13 The NMR spectrum of *N*-Lauroyl-L-phenylalanine (C12-PHE).

CDCl3): δ = 175.38, 174.12, 57.01, 36.67, 31.89, 30.98, 29.59, 29.47, 29.32, 29.30, 29.21, 25.73, 22.67, 18.97, 17.69, 14.10.

N-Lauroyl-L-leucine (C12-LEU)

Mp. = 105.3–105.5 °C.

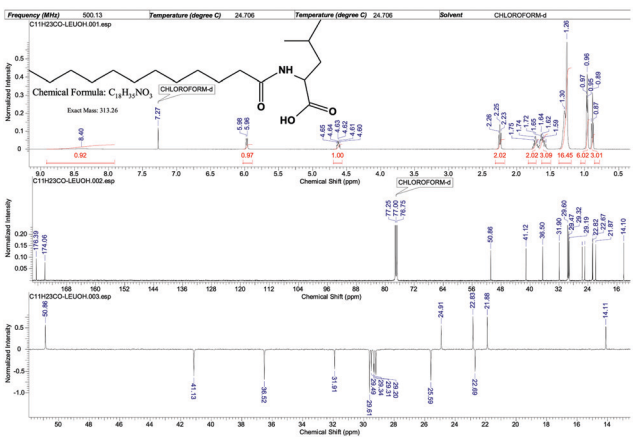

Fig. 11 The NMR spectrum of *N*-Lauroyl-L-leucine (C12-LEU).

^{1}H NMR (500 MHz, $CDCl_3$): δ = 8.40 (bs, 1H), 5.97 (bd, J = 8.2 Hz, 1H), 4.62 (td, J = 8.5 Hz, 1H), 2.26 (t, J = 7.6 Hz, 2H), 1.76–1.68 (m, 2H), 1.76–1.68 (m, 2H), 1.67–1.57 (m, 3H), 1.35–1.25 (m, 16H), 0.96 (t, J = 5.0, 6H), 0.89 (t, J = 6.9, 3H). ^{13}C NMR (125 MHz, $CDCl_3$): δ = 176.39, 174.06, 50.86, 41.12, 36.50, 31.90, 29.60, 29.47, 29.30, 29.19, 25.58, 24.90, 22.82, 22.67, 21.87, 14.10.

N-Lauroyl-L-proline (C12-PRO)

Mp. = 55.1–56.3 °C.

^{1}H NMR (500 MHz, $CDCl_3$): δ = 10.55 (bs, 1H), 4.59 = 4.58 (m, 1H), 3.61–3.57 (m, 1H), 3.50 = 3.45 (m, 1H), 2.41 = 2.33 (m, 3H), 2.10–1.97 (m, 3H), 1.66 (q, J = 7.3, 2H), 1.40–1.20 (m, 16H), 0.88 (t, J = 6.9, 3H). ^{13}C NMR (125 MHz, $CDCl_3$): δ = 59.80, 47.81, 34.48, 31.90, 29.60, 29.47, 29.38, 29.32, 29.31, 27.58, 24.75, 24.54, 22.68, 14.11.

N-Lauroyl-L-phenylalanine (C12-PHE)

Mp. = 97.4–98.6 °C.

^{1}H NMR (500 MHz, $CDCl_3$): δ = 8.45 (bs, 1H), 7.31–7.24 (m, 3H), 7.17–7.15 (m, 2H), 5.99 (dd, J = 13.4, 5.5 Hz, 1H), 3.24

(dd, J = 14.0, 5.5 Hz, 1H), 3.24 (dd, J = 14.0, 5.5 Hz, 1H), 2.18 (m, 2H), 1.60–1.50 (m, 2H), 1.35–1.20 (m, 16), 0.88 (t, J = 6.7 Hz, 3H). ^{13}C NMR (125 MHz, $CDCl_3$): δ = 174.66, 174.00, 135.65, 129.32, 128.64, 127.21, 53.14, 37.22, 36.44, 31.90, 29.32, 29.28, 29.13, 25.52, 22.67, 14.10.

Appendix C (Determination of the acid dissociation constant, K_A)

The values of the acid dissociation constant K_A were determined by the weak acid titration method, using NaOH solution as a strong base.[12] The titration procedure was monitored independently by pH and conductivity determination (see Fig. 14).

The titration process consisted of the gradual addition of NaOH solution from a burette to an Erlenmeyer containing 50 mL of the AAS solution, which was stirred continuously. The initial concentrations of the AASs and base solutions were identical. The experiment was aimed for the determination of the so-called equivalence point (see Fig. 14), at which the concentrations of the dissociated ([A–]) and non-dissociated ([HA]) form of the AAS are identical. To increase the accuracy of the pK_a determination, the equivalence point was approximated using 1st and 2nd derivative of the pH values (Fig. 14A). For conductivity results, the inflection point could be accurately determined from the raw data. The pK_a was determined as half of the equivalence point value, at which, according to the equation the [A–] = [HA], thus pK_a = pH.

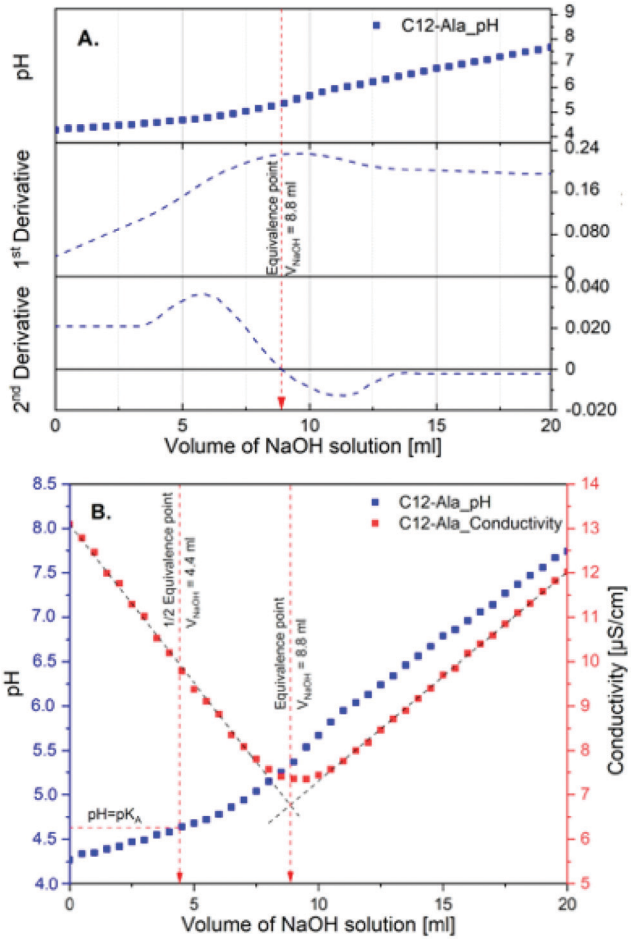

Fig. 14 Graphical determination of pK_a from pH and conductivity data: (A) determination of the equivalence (inflection) point using pH derivatives and (B) determination of the as a half of the inflection point approximated by the pH and conductivity measurements (data for C12-ALA).

Acknowledgements

Partial financial support from the Polish National Science Centre grant number 2019/33/B/NZ7/01608 & 2020/38/E/ST8/00173 is acknowledged with gratitude. The European Union Erasmus+ programme (project number: 2018-1-PL01-KA103-047692) is acknowledged for providing scholarship (financial support) for the research/mobility/traineeship. PW and JZ acknowledges partial financial support of the project by the statutory research fund of ICSC PAS. We also wish to thank John Belanger for proofreading this manuscript.

References

1 J. J. Morelli and G. Szajer, *J. Surfact. Deterg.*, 2000, **3**(4), 539–552.
2 D. B. Tripathy, A. Mishra, J. Clark and T. Farmer, *C. R. Chim.*, 2018, **21**, 112–130.
3 P. Johnson, V. J. Pinfield, V. Starov and A. Trybala, *Adv. Colloid Interface Sci.*, 2021, **288**, 102340.
4 A. Pradhan and A. Bhattacharyya, *J. Clean. Prod.*, 2017, **150**, 127–134.
5 R. Borders and K. Holmberg, *Adv. Colloid Interface Sci.*, 2015, **222**, 79–91.
6 C. N. Mulligan, S. K. Sharma and A. Mudhoo, *Biosurfactants: research trends and applications*. CRC Press, 2019, pp. 352.
7 L. Pérez, M. R. Infante, R. Pons, C. Moran, P. Vinardell, M. Mitjans and A. Pinazo, *Colloids Surf. B*, 2004, **35**(3), 235–242.
8 L. Pérez, A. Pinazo, M. T. García, M. del Carmen Moran and M. R. Infante, *New J. Chem.*, 2004, **28**(11), 1326–1334.
9 N. Wang, K. Yao, Y. Wang, J. Ti, J. Tan, C. Liu, G. Zhang, C. Wang and B. Xu, *J. Surfactants Deterg.*, 2020, **23**, 239–250.
10 A. Pal, Y. K. Ghosh and S. Bhattacharya, *Thetrahedron*, 2007, **63**, 7334–7348.
11 A. Makholf, F. Hubalek and F. A. Foger, WO2014060447A1, 2014.
12 M. Leonard, *Vogel's, Textbook of quantitative chemical analysis. Endeavour*, 5th edn, 1990, 14, 100.
13 E. Helfand, H. L. Frisch and J. L. Lebowitz, *J. Chem. Phys.*, 1961, **34**, 1037.
14 T. Boublik, *Mol. Phys.*, 1975, **29**, 421–428.
15 J. J. Talbot, X. Jin and N.-H. Wang, *Langmuir*, 1994, **10**, 1663–1666.
16 A. Frumkin, *Z. Phys. Chem.*, 1925, **116**, 466.

17 I. B. Ivanov, K. P. Ananthapadmanabhan and A. Lips, *Adv. Colloid Interface Sci.*, 2006, **123-126**, 189–212.
18 A. V. Marenich, C. J. Cramer and D. G. Truhlar, *J. Phys. Chem. B*, 2009, **113**, 6378–6396.
19 B. H. Besler, K. M. Merz and P. A. Kollman, *J. Comput. Chem.*, 1990, **11**(4), 431–439.
20 M. J. Frisch, *Gaussian 09, Revision A.2*, Gaussian, Inc., Wallingford. CT, 2009.
21 E. Krieger and G. Vriend, *J. Comput. Chem.*, 2015, **36**, 996–1007.
22 D. A. Case, V. Babin, J. T. Berryman, R. M. Betz, Q. Cai, D. S. Cerutti, T. E. Cheatham, T. A. Darden, R. E. Duke and H. Gohlke, *et al.*, *AMBER 14*, University of California, San Francisco, CA, USA, 2014.
23 W. Barzyk, K. Lunkenheimer, P. Warszynski, A. Pomianowski and U. Rosenthal, *Prog. Colloid Polym. Sci.*, 2000, **116**, 107–112.
24 K. Lunkenheimer, K. Haage and R. Hirte, *Langmuir*, 1999, **15**, 1052–1058.
25 G. Para, E. Jarek, P. Warszyński and Z. Adamczyk, *Colloids Surf., A*, 2003, **222**(1-3), 213–222.
26 E. Jarek, P. Wydro, P. Warszyński and M. Paluch, *J. Colloids Interface Sci.*, 2006, **293**, 194–202.
27 E. Jarek, T. Jasiński, W. Barzyk and P. Warszyński, *Colloids Surf., A*, 2010, **354**(1-3), 188–196.
28 V. B. Fainerman, V. I. Kovalchuk, E. V. Aksenenko and R. Miller, *Langmuir*, 2016, **32**, 500–5509.
29 J. L. Cornette, K. B. Cease, H. Margalit, J. L. Spouge, J. A. Berzofsky and C. DeLisi, *J. Mol. Biol.*, 1987, **195**, 659–685.
30 A. Mohanty and J. Dey, *Langmuir*, 2007, **23**, 1033–1040.
31 G. Zhao and E. London, *Protein Sci.*, 2006, **15**(8), 1987–2001.
32 W. Qiao and Y. Qiao, *J. Surfactants Deterg.*, 2013, **16**, 821–828.
33 C. Moran, P. Clapes, F. Comelles, T. Garcıa, L. Perez, P. Vinardell, M. Mitjans and M. R. Infante, *Langmuir*, 2001, **17**, 5071–5075.
34 S. Miyagishi, T. Asakawa and M. Nishida, *J. Colloid Interface Sci.*, 1989, **131**, 68–73.
35 M. J. Rosen and J. T. Kunjappu, ed., *Surfactants and interfacial phenomena*, Wiley, Hoboken, NJ, 4th edn, 2012.
36 A. Zdziennicka and B. Janczuk, *J. Mol. Liq.*, 2017, **243**, 236–244.
37 K. Szymczyk, A. Zdziennicka and B. Janczuk, *J. Sol. Chem.*, 2018, **47**, 1824–1840.
38 V. B. Fainerman, S. V. Lylyk, E. V. Aksenenko, M. V. Makievski, J. T. Petkov, J. Yorke and R. Miller, *Colloids Surf., A*, 2009, **334**(1-3), 1–7.

